Journal of Photochemistry and Photobiology A: Chemistry 353 (2018) 159–170

Contents lists available at ScienceDirect

Journal of Photochemistry and Photobiology A: Chemistry

journal homepage: www.elsevier.com/locate/jphotochem

Photocatalytic degradation of terbuthylazine: Modelling of a batch recirculating device

Jérôme Le Cunff[a,*], Vesna Tomašić[b], Zoran Gomzi[b]

[a] Xellia d.o.o., Slavonska avenija 24/6, 10000, Zagreb, Croatia
[b] University of Zagreb, Faculty of Chemical Engineering and Technology, University of Zagreb, Trg Marka Marulića 19, 10000, Zagreb, Croatia

ARTICLE INFO

Article history:
Received 13 August 2017
Received in revised form 12 November 2017
Accepted 13 November 2017
Available online 14 November 2017

Keywords:
Recirculating reactor
Photolytic/photocatalytic degradation
Terbuthylazine
TiO_2/chitosan
Photoreactor
Triazines

ABSTRACT

A thin layer photocatalyst using chitosan to immobilize TiO_2 on a glass fiber woven roving material was successfully used for photocatalytic degradation of terbuthylazine, s model s-triazine herbicide. The reaction was conducted in a photocatalytic recirculating reactor with the photocatalyst inserted as a removable module. The experimental reaction system employed in this study was composed of an annular photoreactor with the immobilized TiO_2/chitosan layer and the radiation source and the second part of the reaction system only used for the aeration or the reaction mixture, both operating in unsteady conditions. The kinetic model is based on a simplified consecutive degradation of terbuthylazine to cyanuric acid through intermediate products. The model of the annular reactor is represented by a hyperbolic partial differential equation solved by method of characteristics; the model of the aeration vessel is given by an ordinary differential equation. The proposed model represents a simple way to describe a complex recirculating reactor system operating in unsteady conditions.

1. Introduction

Persistent organic pollutants (POPs), like pesticides, are not easily degraded by conventional degradation methods, making advanced oxidation processes like photocatalysis increasingly interesting to many researchers [1–6].

Research on photocatalysis is mostly based on TiO_2 suspended nanoparticles in fluid phase contaminated with organic pollutants, allowing for the largest surface area and efficient photocatalytic degradation. The lack of the photocatalysts selectivity allows a very wide range of their application [7–12]. Retrieval or separation of suspended photocatalytic nanoparticles from the fluid phase is the major drawback of this process [13–16]. Regeneration is also a challenge in the case of suspended nanoparticles making the photocatalyst poisoning another issue, as well environmental contamination [17–21].

Immobilization of TiO_2 is a common way to solve these issues [17,22]. The specific surface of a thin layer is very small compared to the reactor, which can, including the external mass transfer limitations, lead to a 70% reduction in photocatalyst performance compared to the suspension reactors. Immobilized layers offer the possibility of easier photocatalyst modifications, as well as regeneration [17,23–28]. Regardless, for industrial application, the photocatalyst needs to be removable, allow easy maintenance and off site regeneration. It also needs to withstand harsh operating conditions of industrial water and prepared from easily available and cost effective materials, also avoiding the risk of additional pollution. TiO_2 and chitosan as the photocatalyst binder are quite common and widely available materials, suited for such applications [29–42].

This study presents the development of a mathematical model of the photocatalytic recirculating reactor with an immobilized photocatalytic layer described in a previous paper [43]. The experimental reaction system comprised two parts. An annular photoreactor, with the immobilized TiO_2/chitosan layer and the central radiation source. Since process variables were not only time dependent, but also dependent on the position along the reactor length, the reaction system could not be considered homogenous and solved as a batch reactor as it is usually done [44,45]. The annular part of the reactor system was described using a hyperbolic differential equation. The equation was simplified by variable substitution, expressing both the reactor length and reaction time as the residence time with the Courant number being equal to 1. The second part of the system was used for aeration of

* Corresponding author.
E-mail address: jerome.le-cunff@xellia.com (J.L. Cunff).

https://doi.org/10.1016/j.jphotochem.2017.11.020
1010-6030/

Nomenclature

Symbols

A_r	Frequency factor, min^{-1}
c_0	Initial concentration of terbuthylazine, mg dm^{-3}
$c_{(CYA)}$, $c_{(MP)}$, $c_{(TBA)}$	Concentration of the indicated compounds, mg dm^{-3}
c_i	Concentration of compound *i*, mg dm^{-3}
E_a	Activation energy, kJ mol^{-1}
k_1, k_2	Reaction rate constants (Eq. (1)), min^{-1}
n	Order of the reaction, dimensionless
Q_R	Recirculation flow rate, $dm^3\ min^{-1}$
Q_A	Aeration flow rate, $dm^3\ min^{-1}$
r_{TBA},	Rate of reactant consumption
r_{MP}, r_{CYA}	Rate of the intermediate products or reaction product formation (Eqs. 2–4), g $dm^{-3}\ min^{-1}$
RMSD	Root mean square deviation, dimensionless
R^2	Correlation coefficient, dimensionless
t	Irradiation time, min
T	Reaction temperature, °C
u	Linear velocity of the solution, dm min^{-1}
v_0	Volumetric flow, $dm^3\ min^{-1}$
V_m	Volume of the aeration vessel, dm^3
V_r	Total volume of the reactor, dm^3
X_{TBA}	Terbuthylazine conversion, %
$Y_{CYA,\ TBA}$	the reaction yield of cyanuric acid, %
z	Axial position along the length of the reactor, dm

Greek letters

ρ	Volume density of the catalyst, $g_{cat}\ dm^{-3}$
τ	Residence time of the reaction mixture, min
τ_m	Residence time of the reaction mixture in the aeration vessel, min
$\tau_{r,}$	Total residence time of the reaction mixture in the annular reactor, minDAD diode array detector

Abbreviations

CYA	Cyanuric acid
DAD	Diode array detector
DPA	6- deisopropylatrazine (6-chloro-N^2-ethyl-1,3,5-triazine-2,4-diamine according to IUPAC)
DTB	Desethylterbuthylazine (6-chloro-N^2-(tert-butyl)-1,3,5-triazine-2,4-diamine according to IUPAC)
HPLC	High performance liquid chromatography
LC/MS	Liquid chromatography mass spectrometry
MP	Intermediate products
PHCD	Photocatalytic degradation
PHL	Photolytic degradation
TBA	Terbuthylazine
TDA	Acetamideterbuthylazine (N-(4-(tert-butylamino)-6-chloro-1,3,5-triazin-2-yl)acetamide according to IUPAC)
TBH	Hydroxyterbuthylazine (4-tert-butylamino-6-ethylamino-[1,3,5]triazin-2-ol according to IUPAC)

the reaction mixture without any photocatalyst. This part can be approximated as a mixed flow stirred-tank operating in unsteady state. Since process variables were not only time dependent, but also dependent on the position along the reactor length, the reaction system could not be considered homogenous.

2. Experimental set up

2.1. The batch recirculating photocatalytic device

Photocatalytic degradation experiments were carried out using a custom made batch recirculating photocatalytic device presented in Fig. 1. The outer walls of the reactor, as well as the heat exchanging shell, were made of borosilicate glass tubes (i.d. 6 cm). The inner tube was a removable quartz cuvette (o.d. 2.5 cm, cutoff at 195 nm). An *Osram Puritec germicidal HNS G5* lamp (8W, 254 nm) was axially mounted inside the quartz cuvette and centered along the entire length of the photoreactor. The terminal ends of the bulb were blackened with Teflon tape in order to ensure uniform emission of radiation. The other part of the reactor setup was a vessel used for aeration of the reaction solution using controlled air flow from an air compressor. Recirculation of the reaction solution was driven by a peristaltic pump (*Gilson, Model Miniplus Evolution*) and a thermostatic flow bath (*Julabo, Model ED – Heating Immersion Circulator*) was used to ensure isothermal conditions inside the reactor. The photocatalyst module consisted of a thin TiO_2/chitosan layer deposited on the commercial glass fiber woven roving material (*KELTEKS, RT 360*) and mounted on an inox steel frame. The photocatalytic module was placed closed to the inner side of the outside reactor walls facing inwards. The preparation of the photocatalyst layer was described in our previous paper [43].

The thermostatized reaction mixture was recirculated through the reactor system until adsorption equilibrium of the model component on the photocatalyst. The reactor effluent was analyzed as described elsewhere [43] to determine concentration of terbuthylazine and degradation products. Place and sampling intervals were chosen to ensure adequate data for the mathematical model validation. Experiments were conducted until complete degradation of terbuthylazine was achieved, which took up to 120 min.

2.2. Identification of the reaction intermediates

In order to confirm one of the possible reaction mechanisms of terbuthylazine degradation some products of the photocatalytic degradation were identified using LC/MS on samples normally used to monitor the progress of reaction, which were otherwise analyzed on HPLC [43]. The identification was conducted on an *Agilent 1260 HPLC* system with a DAD detector coupled with an *Agilent 6420 QQQ* mass spectrometer. Representative samples from degradation experiments were used for degradation products identification by measuring the molar mass of compounds compared to already known degradation products. The relative retention times were confirmed on the DAD detector before the MS detector for correlation. The retention time of cyanuric acid was identified using the pure substance.

3. Results and discussion

3.1. Identification the intermediate products formed in the photocatalytic and photolytic degradation of terbuthylazine

Using the LC/MS analysis, the following degradation products were identified and subsequently quantified using HPLC in the experiments (Fig. 2): 6-deisopropylatrazine (DPA), desethylterbuthylazine (DTB), acetamideterbuthylazine (TDA) and hydroxyterbuthylazine (TBH).

Compounds illustrated in Fig. 2a–c (hereafter called DPA, DTB i TDA) are specific for a photocatalytic reaction leading to a

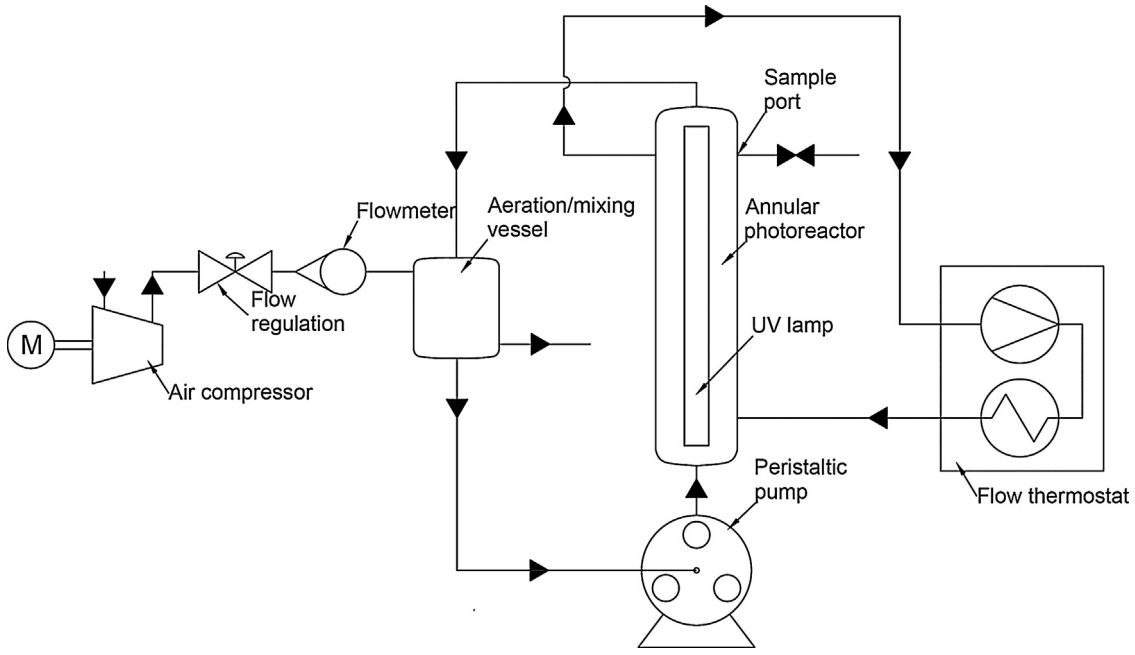

Fig. 1. Schematic diagram of the batch recirculating photocatalytic device.

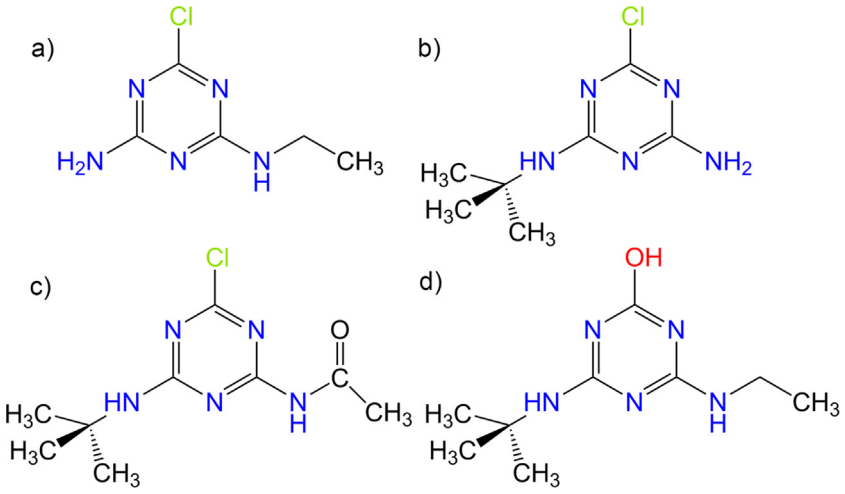

Fig. 2. Intermediate products of terbuthylazine degradation identified using LC–MS: a – DPA, b – DTB, c – TDA, d – TBH.

predominant dealkylation of lateral chains by hydroxyl radicals followed later on by dechlorination. Hydroxylation of terbuthylazine is the dominant degradation mechanism when only UV light is used, leading to the formation of the compound shown in Fig. 2d (hereafter called TBH) [43].

3.2. Influence of different experimental reaction variables on the photocatalytic degradation rate

3.2.1. Influence of recirculation rate

Time required reaching the terbuthylazine adsorption equilibrium on the surface of the photocatalyst before the degradation reaction was determined at different recirculation rates. Terbuthylazine adsorption on the photocatalyst surface becomes more efficient increasing the recirculation rate of the reaction feed corresponding to thickness changes of the boundary layer decreasing mass transfer resistance. Terbuthylazine adsorption was the most intensive during the initial 30 min. At the recirculation rate of 300 $cm^3\,min^{-1}$ the concentration of terbuthylazine decreased from the initial 5 $mg\,dm^{-3}$ to 3.93 $mg\,dm^{-3}$ during that time and only to 3.86 $mg\,dm^{-3}$ during the next 30 min (Fig. 3). Based on these results all degradation experiments were conducted after 30 min "in the dark" (UV lamp off) at the appropriate recirculation rate and reaction temperature.

3.2.2. Comparison of the photolytic and photocatalytic degradation of terbuthylazine

Photolytic degradation of terbuthylazine with UV-C light only is already reported [46]. To evaluate the photolytic contribution to the degradation, experiment were performed in the same reaction conditions ($T = 25\,°C$, $pH = 5$, $Q_R = 300\,cm^3\,min^{-1}$) in the presence and absence of the photocatalyst. As shown in Fig. 4 change in the terbuthylazine concentration during the photolytic degradation was similar compared to the photocatalytic terbuthylazine degradation, indicated that at 254 nm the rate of the photocatalytic reaction is negligible compared to photolysis. However, the

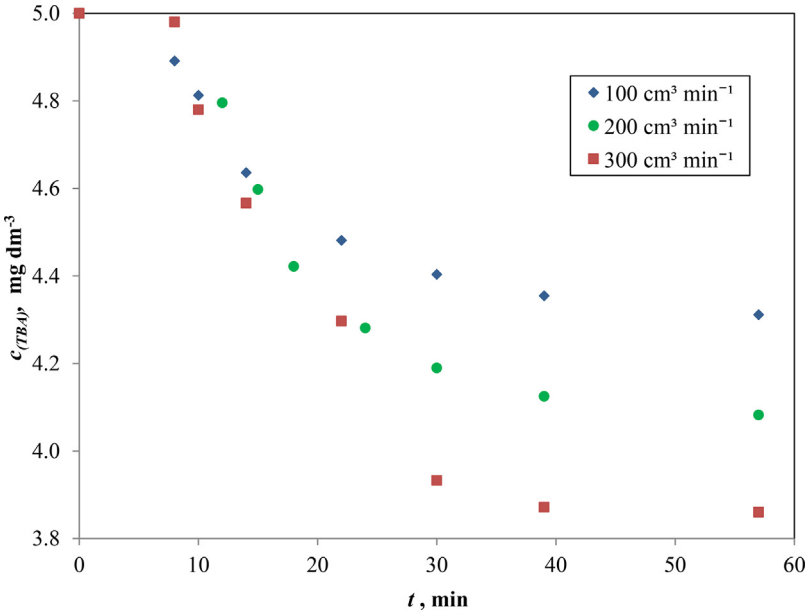

Fig. 3. Influence of recirculation rate on the evolution of terbuthylazine, $c_{(TBA)}$ "in the dark" (Conditions: $c_{0,TBA} = 5\ mg\ dm^{-3}$, T = 25 °C, pH = 5).

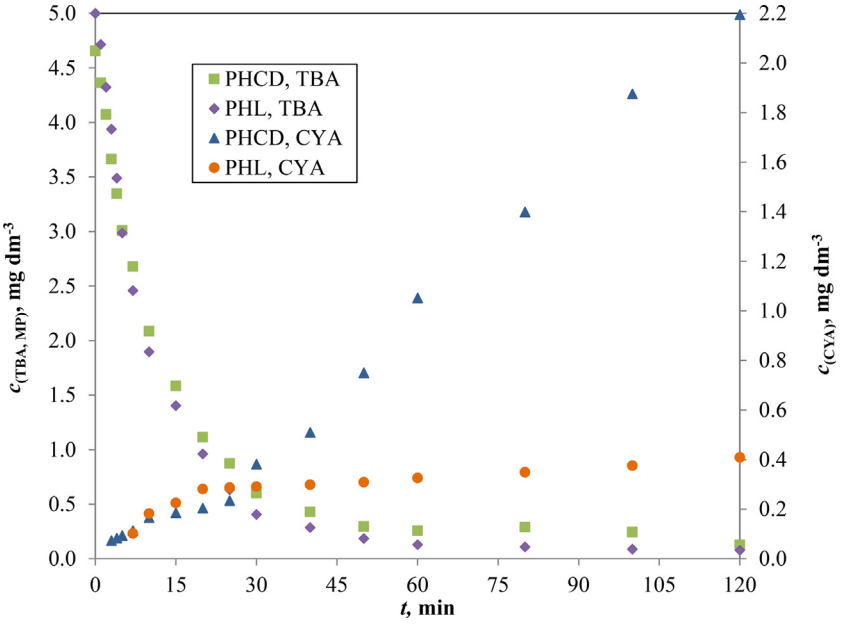

Fig. 4. Comparison of photocatalytic (PHCD) and photolytic (PHL) degradation of terbuthylazine, $c_{(TBA)}$ with the corresponding evolution of the cyanuric acid, $c_{(CYA)}$ (Conditions: $c_{0,TBA} = 5\ mg\ dm^{-3}$, T = 25 °C, $Q_R = 300\ cm^3\ min^{-1}$, pH = 5).

difference was much more pronounced when the final degradation product, cyanuric acid was considered (Fig. 4). As was mentioned previously, the photolytic degradation leads to the formation of TBH by hydroxylation of terbuthylazine, but the subsequent dealkylation of the side chains is much slower resulting in very low reaction yield on cyanuric acid (14.56%). TBH is also generated in the photocatalytic reaction, leading to a similar degradation rate, but with hydroxyl radicals the intermediate products are more easily dealkylated, leading in much higher yields of the cyanuric acid (78.13%).

3.2.3. Influence of the temperature

Temperature did not have significant effects on the degradation of terbuthylazine in the observed reaction system. Due to the UV-C lamp the possible effect of temperature on the reactant adsorption and product desorption is masked by the photolytic contribution (Fig. 5). We can observe a more pronounced influence of temperature on the formation of the cyanuric acid (Fig. 6). The influence of temperature on the formation of cyanuric acid (yield from 78.13% to 91.67% (Table 1) can be explained looking at the evolution of the intermediate products of the reaction, e.g. TBH. At 25 °C the difference in the rates of TBH formation and TBH degradation leads to the maximal concentration of TBH at approximately 80 min (Fig. 7). From 35 to 65 °C the time dependent changes of TBH concentrations are quite similar, however at 75 °C the TBH concentration was below the quantification limit. These results indicate that the reaction temperature has a significant

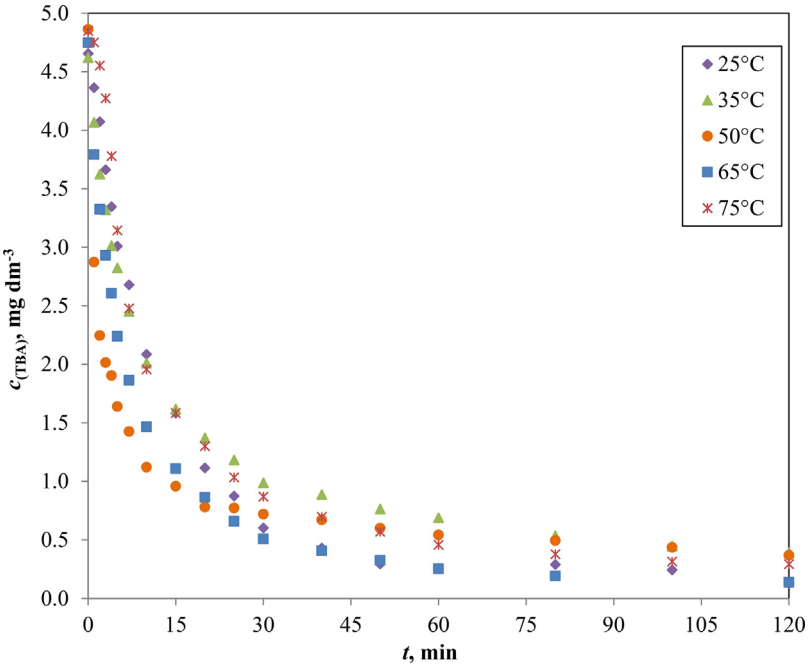

Fig. 5. Photocatalytic degradation of terbuthylazine, $c_{(TBA)}$ at different temperatures (Conditions: $c_{0,TBA} = 5\ mg\ dm^{-3}$, $Q_R = 300\ mL\ min^{-1}$, pH = 5).

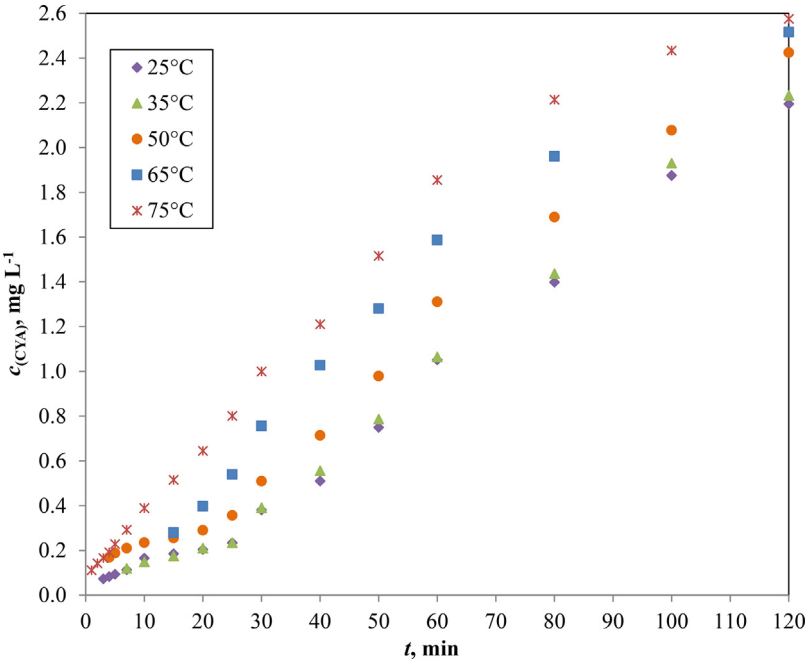

Fig. 6. Evolution of the cyanuric acid, $c_{(CYA)}$ at different temperatures (Conditions: $c_{0,TBA} = 5\ mg\ dm^{-3}$, $Q_R = 300\ mL\ min^{-1}$, pH = 5).

Table 1
Influence of temperature (Conditions: $c_{0,TBA} = 5\ mg\ dm^{-3}$, $Q_R = 300\ mL\ min^{-1}$, pH = 5).

T,°C	X_{TBA}, %	$Y_{CYA,TBA}$, %
25 °C	97.46	78.13
35 °C	92.16	79.84
50 °C	92.62	86.30
65 °C	97.22	89.55
75 °C	94.15	91.67

influence on the degradation of some intermediate reaction products leading to different dominant degradation pathways.

Due to the photolytic influence mentioned before, the effect of recirculation rate is also very difficult to evaluate during the degradation reaction. It was demonstrated previously that increasing the recirculation rate of the reaction feed had significant influence on the adsorption of terbuthylazine. Meanwhile, according to the results shown in Fig. 8 the most progressive photocatalytic degradation of terbuthylazine was achieved at the recirculation rate of $50\ cm^3\ min^{-1}$, especially during the first 10 min of reaction, which corresponds to the maximal residence time of the reactant in the annular part of the reactor. In the case of

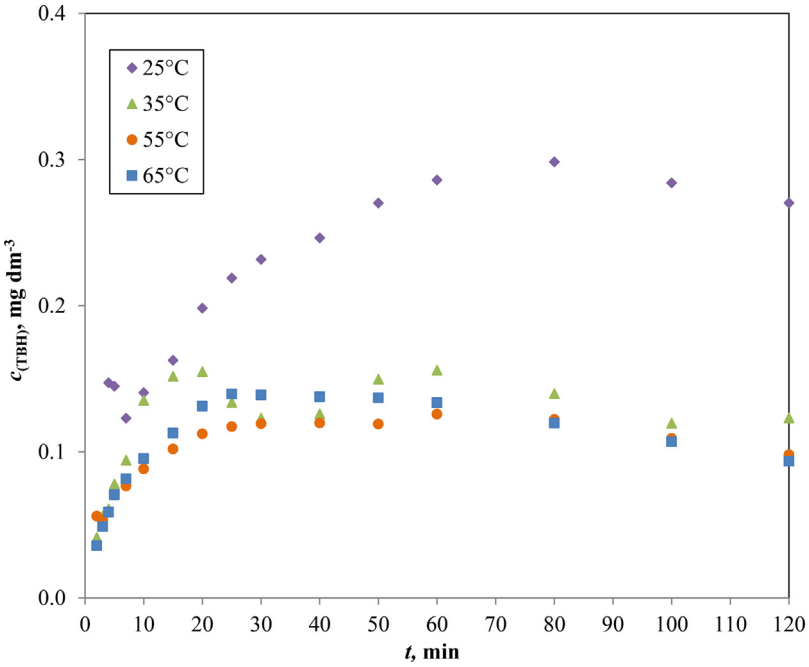

Fig. 7. Evolution of hydroxy-terbuthylazine, $c_{(TBH)}$ at different temperatures (Conditions: $c_{0,TBA} = 5$ mg dm^{-3}, $Q_R = 300$ mL min^{-1}, pH = 5).

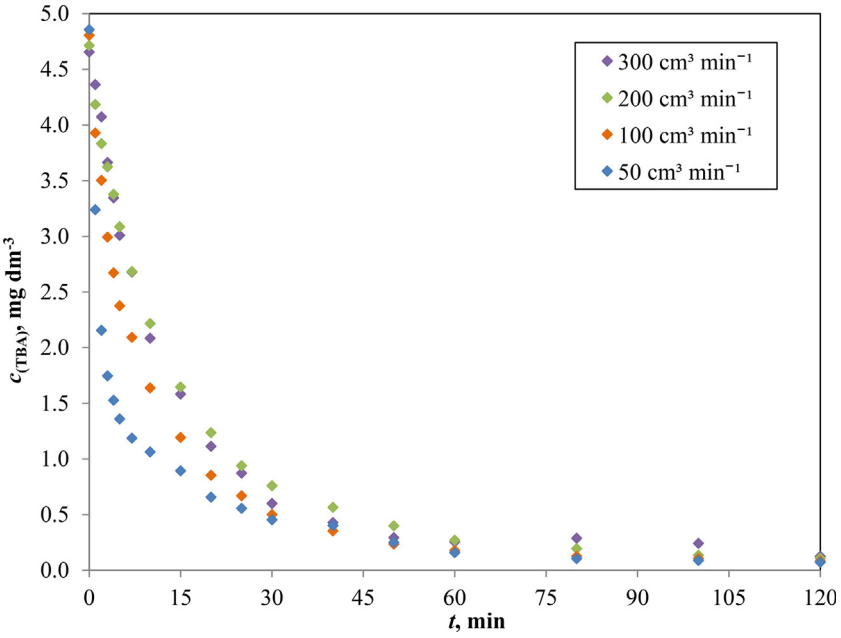

Fig. 8. Photocatalytic degradation of terbuthylazine, $c_{(TBA)}$ at different recirculation rates (Conditions: $c_{0,TBA} = 5$ mg dm^{-3}, T = 25 °C, pH = 5).

terbuthylazine degradation at slower recirculation rate the positive effect of photolysis due to higher residence time probably compensates the effects on photocatalysis. When it comes to the complete degradation, the overall degradation efficiency depends on the efficiency of the photocatalytic reactions. Small change in the concentration of the cyanuric acid as a function of reaction time was observed in the range of recirculation rates from 50 to 100 cm^3 min^{-1} (Fig. 9). However, the higher concentrations and yields of cyanuric acid were experimentally measured at the higher recirculation rates of the reaction feed (Fig. 9, Table 2). These results indicate that the rate of the photocatalytic degradation is highly dependent on the external mass transfer, or the boundary layer thickness.

3.2.4. Influence of the reaction mixture aeration on the efficiency of terbuthylazine degradation

The undesired electron-hole recombination in the absence of proper electron acceptor or donor is known as one of the practical problems in TiO_2 photocatalysis. One approach to inhibit the electron-hole pair recombination is to add an external oxidant or other electron acceptors to the reaction system. In this study aeration of the reaction system was used for this purpose. The influence of the air flow rate during aeration of the reaction mixture on the conversion of terbuthylazine is shown in Table 3. It can be seen that the yield of cyanuric acid and efficiency of the photocatalytuic degradation increases with the flow rate of compressed air.

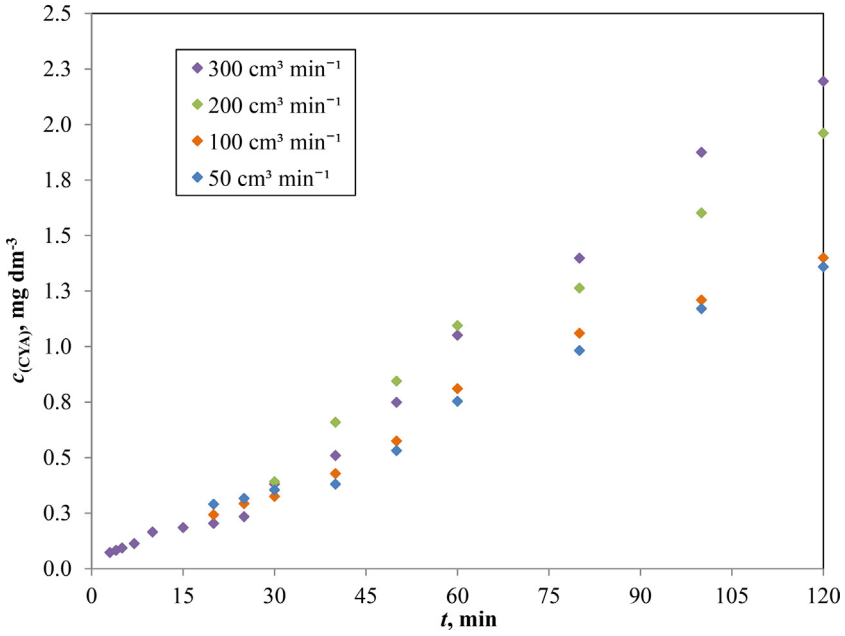

Fig. 9. Evolution of cyanuric acid, $c_{(CYA)}$ at different recirculation rates (Conditions: $c_{0,TBA} = 5\ mg\ dm^{-3}$, T = 25 °C, pH = 5).

Table 2
Effect of the recirculation rate (Reaction conditions: $c_{0,TBA} = 5\ mg\ dm^{-3}$, T = 25 °C, pH = 5).

Q_R, $cm^3\ min^{-1}$	X_{TBA},%	$Y_{CYA,TBA}$,%
50	98.52	48.38
100	98.29	49.83
200	97.80	69.80
300	97.46	78.13

Table 3
Effect of the compressed air flow rate (Reaction conditions: $c_{0,TBA} = 5\ mg\ dm^{-3}$, T = 25 °C, pH = 5; $Q_R = 300\ cm^3\ min^{-1}$).

Q_A, $mL\ min^{-1}$	X_{TBA},%	$I_{CYA,TBA}$,%
0	97,46	78,13
100	98,48	86,41
200	95,91	91,31
300	93,61	94,46
400	98,44	97,63

The flow rate of air during aeration of the reaction mixture has significant influence on the formation/degradation of TBH, demonstrating the effect on the photocatalytic reaction. Obviously, aeration is a cheap and easy approach preventing the electron-hole recombination to ensure efficient photocatalysis. It is also more acceptable in water treatment processes, in contrast to other electron acceptors such as bromates, thiosulfates or hydrogen peroxide (Fig. 10).

3.3. Development and validation of the proposed mathematical model

Photocatalytic degradation is proven to be a very complex reaction involving a great number of possible intermediate products and degradation pathways [43]. To simplify the mathematical model the reaction can be described as a simplified consecutive reaction of terbuthylazine degradation to cyanuric acid through intermediate products:

$$C_9H_{16}ClN_5 + O_2 \xrightarrow{k1} \text{interm. prod.} \xrightarrow{k2} C_3H_3N_3O_3 + CO_2 + Cl^- + H_2O + NH_3 \quad (1)$$

As described previously, terbuthylazine photocatalysis was performed using the laboratory scale experiments. The experimental photoreaction device consists of two parts: the annular photoreactor and the aeration/mixing vessel. Photocatalysis is taking place in the annular photoreactor over the immobilized photocatalytic layer placed close to the inner wall. The lamp is located inside a transparent photoreactor tube in the central position providing a symmetric irradiation field. The annular photoreactor was a part of a closed recirculated system. However, it cannot be considered as batch reactor due to concentration differences along the length of the reactor, as confirmed by experiments, but as a plug-flow reactor. The second part of the experimental system is a vessel used for aeration and mixing of solution. There is no photoreaction in this part, but it also operates in unsteady state. The concentrations of terbuthylazine and cyanuric acid recorded during degradation experiments at the exit of reactor were used for model validation. The results showed that there was a significant difference in concentrations from the entry to the exit of the annular reactor, therefore small conversions could not be assumed. Accordingly, the whole reaction system consists of an annular reactor operating in unsteady conditions, connected in series with a vessel used for aeration and mixing also operating in unsteady conditions. Fig. 11 shows the schematic representation of the experimental system used to develop the model.

The overall model of the reactor system, consisting of a model of an annular flow reactor and the model of the aeration vessel as two subsystems connected in series by the inlet and outlet flows of the reaction solution. Following characteristics of the experimental system were assumed and used during the development of the model:

1. ideal flow through the annular photoreactor
2. ideal mixing in the aeration vessel
3. the outlet concentration of the annular reactor at a specific time is also the inlet concentration in the aeration vessel,
4. the outlet concentration of the aeration vessel is at the same time the inlet concentration of the annular reactor,
5. for every subsequent time point, $t + \Delta t$ the concentration profile down the length of the reactor needs to be recalculated in order

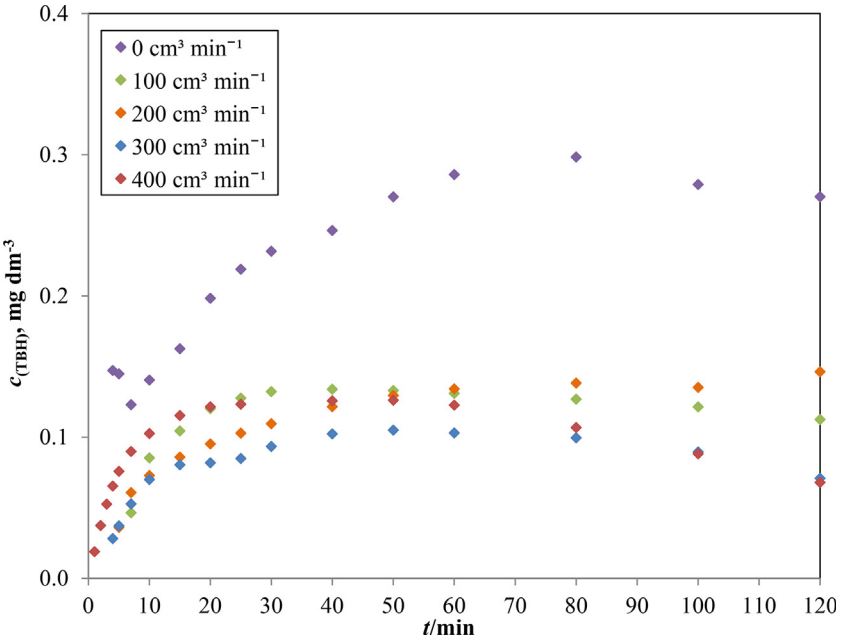

Fig. 10. Evolution of hydroxy-terbuthylazine, $c_{(TBH)}$ as a function of the compressed air flowrate during aeration of the reaction mixture. (Conditions: $c_{0,TBA} = 5\,mg\,dm^{-3}$, T = 25 °C, $Q_R = 300\,cm^3\,min^{-1}$, pH = 5).

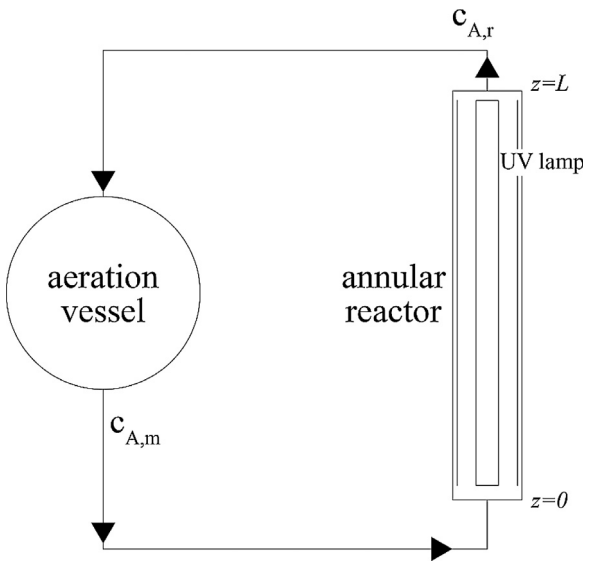

Fig. 11. Schematic of the reaction system.

to determine the outlet concentration of the reactor, also the inlet concentration of the aeration vessel.

3.3.1. Kinetic model

The sequential reaction described in Eq. (1) can be written using the following kinetic models:

$$r_{TBA} = \rho k_1 c_{TBA,r}^{n} \tag{2}$$

$$r_{MP} = \rho k_1 c_{TBA,r}^{n} - \rho k_2 c_{MP,r} \tag{3}$$

$$r_{CYA} = \rho k_2 c_{MP,r} \tag{4}$$

In the Eqs. (2)–(4), ρ is the volume density of the catalyst (g_{cat} dm^{-3}) and $c_{TBA,r}$, $c_{MP,r}$ are the concentrations of terbuthylazine and intermediate products, respectively. The order of the reaction, exponent n, with respect to the reactant equals to 1.5, while the formation of cyanuric acid is a first order reaction. Those values were determined as parameters by testing the whole model system with experimental data.

3.3.2. Reactor model

Based on these assumption the model of the unsteady state annular reactor is described with Eq. (5), including the kinetic model, Eq. (2). Only Eq. (2) was used to demonstrate the model as the same principles apply for Eq. (3) and (4).

$$u\frac{\partial c_{TBA,r}}{\partial z} - \frac{\partial c_{TBA,r}}{\partial t} + \rho k_1 c_{TBA,r}^{1.5} = 0 \tag{5}$$

Eq. (5) represents a hyperbolic partial differential equation that can be solved numerically by the method of characteristics [47] leading to a simpler ordinary differential equation:

$$\frac{dc_{TBA,r}}{d\tau} + \rho k_1 c_{TBA,r}^{1.5} = 0 \tag{6}$$

The new variable τ represents the residence time along the length of the reactor defined by the following equation

$$\tau = \frac{z}{u} \tag{7}$$

where z represents an axial position down the length of the reactor and u represents the linear velocity of the solution ($m\,s^{-1}$). Eq. (6) is solved for the residence time interval from $\tau = 0$ to τ_r, the total residence time in the annular reactor.

$$\tau_r = \frac{V_r}{v_0} \tag{8}$$

V_r is the total volume of the reactor (dm^3) and v_0 represents the volumetric flow ($dm^3\,s^{-1}$). Eq. (6) can be solved by numerical methods, but there is an analytical solution for order of 1.5. For each time step the inlet and outlet concentrations of the annular reactor change, as well as those of the aeration vessel. The outlet

concentration of the aeration vessel is also the inlet concentration of the annular reactor, and for each new inlet concentration of the annular reactor a new concentration profile is calculated, down the length of the reactor or along the residence time.

The differential equation, Eq. (6) was solved for *i*-th time from $c_{TBA,r}(i,j-1)$ to $c_{TBA,r}(i,j)$ in the interval of residence time from $\tau(0)$ to $\tau(M)$. Following those boundary and initial conditions, the concentration inside the annular reactor can be determined using the following equation:

$$c_{TBA,r}(i,j) = \left(\frac{1}{0,5\cdot\rho\cdot k\cdot\Delta\tau\cdot j+\frac{1}{\sqrt{c_{TBA,m}(i-1)}}}\right)^2 \tag{9}$$

For the time i the concentration is calculated for the residence times ranging from $j=0$ to $j=M$, (from $\tau=0$ to τ_r). The final outlet concentration for the time $t+\Delta t$, is equal to:

$$c_{TBA,r}(t+\Delta t,\tau) = \left(\frac{1}{0,5\cdot\rho\cdot k\cdot\tau+\frac{1}{\sqrt{c_{TBA,m}(t)}}}\right)^2 \tag{10}$$

Eq. (10) can also be written as:

$$c_{TBA,r}(i,M) = \left(\frac{1}{0,5\cdot\rho\cdot k\cdot\tau\cdot M+\frac{1}{\sqrt{c_{TBA,m}(i-1)}}}\right)^2 \tag{11}$$

The outlet concentration from the annular reactor, Eq. (11) is also the inlet concentration of the aeration vessel at the time *i*. This concentration was measured during the degradation experiments and used for the estimation of the model parameters and validation of the model.

3.3.3. Model of the aeration vessel

The model of the aeration vessel operating in unsteady state and without photoreactions is represented by the following equation for Eq. (2),

$$V_m\frac{dc_{TBA,m}}{dt} = c^u_{TBA,m}v_0 - c^{iz}_{TBA,m}v_0 \tag{12}$$

where V_m is the volume of the aeration vessel, v_0 is the volumetric flow while $c^u{}_{TBA,m}$ and $c^{iz}{}_{TBA,m}$ are the inlet and outlet concentrations of the aeration vessel. Eq. (12) can be reorganized in the following manner: since the volume of the aeration vessel is constant the outlet concentration is also the concentration inside the vessel, $c^{iz}{}_{TBA,m} = c_{TBA,m}$:

$$\tau_m\frac{dc_{TBA,m}}{dt} = c^u_{TBA,m} - c_{TBA,m} \tag{13}$$

The ordinary differential equation, Eq. (13) also has an analytical solution. The boundary conditions from $c_{TBA,m}(t-\Delta t)$ to $c_{TBA}(t)$ actually ranging from the time $t-\Delta t$ to t. The solution, according to the boundary conditions is:

$$c_{TBA,m}(t) = c^u_{TBA,m}(t) + \left(c_{TBA,m}(t-\Delta t) - c^u_{TBA,m}(t)\right)\exp\left(-\frac{\Delta t}{\tau_m}\right) \tag{14}$$

or, using the coefficient *i*, for values at time $t+\Delta t$

$$c_{TBA,m}(i) = c^u_{TBA,m}(i) + \left(c_{TBA,m}(i-1) - c^u_{TBA,m}(i)\right)\exp\left(-\frac{\Delta t}{\tau_m}\right) \tag{15}$$

Since the inlet concentration of the aeration vessel is also the outlet concentration of the annular reactor, the last equation can be written as:

$$c_{TBA,m}(i) = c_{TBA,r}(i,M) + \left(c_{TBA,m}(i-1) - c_{TBA,r}(i,M)\right)\exp\left(-\frac{\Delta t}{\tau_m}\right) \tag{16}$$

The inlet concentration of the annular reactor at the next time period $t+\Delta t$, *i.e.* at the step i + 1 is equal to the outlet concentration of the aeration vessel in the same time period, $c_{TBA,r}(i+1,0) = c_{TBA,m}(i+1)$. Since there are no chemical reactions occurring in the aeration vessel, the analytical solution of Eq. (16) is also used to calculate the concentrations of the intermediate products and the final product.

3.3.4. Model of the complete reactor system

The mathematical model of the complete closed recirculation system, comprising a model of an annular reactor and a model of the aeration vessel, can be described by the following set of material balances for all constituents in the reaction path, Eqs. (2)–(4).

1. The boundary and initial conditions at the inlet of the annular reactor are:

$$c_{TBA,r}(i+1,0) = c_{TBA,m}(i+1) \tag{17}$$

$$c_{MP,r}(i+1,0) = c_{MP,m}(i+1) \tag{18}$$

$$c_{CYA,r}(i+1,0) = c_{CYA,m}(i+1) \tag{19}$$

2. Concentrations of terbuthylazine (TBA), the intermediate products (represented as the sum) (MP) and the cyanuric acid (CYA) inside the annular reactor are calculated from the system of balances, Eqs. (20)–(22),

$$\frac{dc_{TBA,r}}{d\tau} = -\rho k_1 c^{1,5}_{TBA,r} \tag{20}$$

$$\frac{dc_{MP,r}}{d\tau} = \rho k_1 c^{1,5}_{TBA,r} - \rho k_2 c_{MP,r} \tag{21}$$

$$\frac{dc_{CYA,r}}{d\tau} = \rho k_2 c_{MP,r} \tag{22}$$

3. The new boundary conditions at the outlet of the annular reactor and at the inlet of the aeration vessel

$$c^u_{TBA,m}(i+1) = c_{TBA,r}(i+1,M) \tag{23}$$

$$c^u_{MP,m}(i+1) = c_{MP,r}(i+1,M) \tag{24}$$

$$c^u_{CYA,m}(i+1) = c_{CYA,r}(i+1,M) \tag{25}$$

Following the previous statements the outlet concentration of the annular reactor, is the solution for each of the differential equations, Eqs. (23)–(25) for the position $j=M$, or the last residence time of the reactor, τ_r.

4. Concentrations of terbuthylazine, intermediate products and cyanuric acid are calculated from the analytical solution of differential equations representing material balances inside the

aeration vessel, Eqs.(26)–(28)

$$c_{TBA,m}(i+1) = c_{TBA,r}(i+1,M) + (c_{TBA,m}(i) - c_{TBA,r}(i+1,M))\exp\left(-\frac{\Delta t}{\tau_m}\right) \quad (26)$$

$$c_{MP,m}(i+1) = c_{MP,r}(i+1,M) + (c_{MP,m}(i) - c_{MP,r}(i+1,M))\exp\left(-\frac{\Delta t}{\tau_m}\right) \quad (27)$$

$$c_{CYA,m}(i+1) = c_{CYA,r}(i+1,M) + (c_{CYA,m}(i) - c_{CYA,r}(i+1,M))\exp\left(-\frac{\Delta t}{\tau_m}\right) \quad (28)$$

The material balance equations for the annular reactor, Eqs. (20)–(22), and the material balance equations for the aeration vessel, Eqs. (26)–(28), are mutually connected by boundary conditions, Eqs. ((17)–(19) and (23)–(25)). To solve those equations we need to set initial conditions and the corresponding parameters, k_1 and k_2 in the equations, Eqs. (20)–(22).

The initial conditions for the reaction system at time $t = 0$ are the following:

$$c_{TBA,m}(0) = c_{TBA,0} \text{ i } c_{TBA,r}(0,j) = c_{TBA,0} \quad (29)$$

$$c_{CYA,m}(0) = c_{MP,m}(0) = 0 \text{ i } c_{CYA,r}(0,j) = c_{MP,r}(0,j) = 0 \quad (30)$$

where $c_{TBA,0}$ is the initial concentration of the reactant terbuthylazine, while c_{MP} and c_{CYA} are the concentrations of the intermediate products and cyanuric acid. The subscript m corresponds to the aeration vessel, and the subscript r to the annular reactor. The concentrations of the intermediate product and cyanuric acid for the time $t = 0$ is 0 mg dm^{-3}.

3.3.5. Model validation

The validation of the model was conducted by fitting experimental data for terbuthylazine and cyanuric acid obtained during degradation experiments with theoretical data predicted by the proposed model. Since one of the material balance equations did not have an analytical solution, Eq. (21), Runge Kutta IV was used. The only adjustable parameters of the model were the reaction rate constants k_1 and k_2, Eqs. (20)–(22). The Nelder-Mead method of nonlinear optimization was used for the parameter estimation with root mean square deviation, RMSD, Eq. (31) as determination criteria:

$$RMSD = \frac{1}{\sum_{i=1}^{i=2} N_i}\sqrt{\sum_{i=1}^{i=2}\sum_{j=1}^{j=N_i}\left(y_{i,j(theor.)} - y_{i,j(exp.)}\right)^2} \quad (31)$$

where N_i represents the total number of measured data of the component i, while j indicates the number of the measured data. The data for terbuthylazine and cyanuric acid obtained experimentally were compared to the values obtained by solving the model equations.

The program used for model validation was written using *Matlab 7.0 (R14)*. Examples of the fit of the model are given in Fig. 12 As can be seen from Fig. 12, the model is able to describe the trend of the experimental data very well, meaning that the proposed model can be applied to describe the overall reaction system. The figure shows a simulation of the reaction intermediates profiles (MP – sum of intermediate products) without corresponding experimental data, since only several were quantified. The profile of MP is reaching a maximum concentration at the moment where terbuthylazine degradation slows down.

The effect of temperature on the reaction rate was evaluated using the Arrhenius equation. The frequency factor A_r and the apparent activation energy E_a were determined using rate constants obtained from the mathematical model for different temperatures (Table 4).

Activation energies for both reactions are very low, only 12.88 kJ mol^{-1} for terbuthylazine degradation of and a value near zero for cyanuric acid formation. The results support the assumption that the rate of photocatalytic degradation of terbuthylazine is almost independent of temperature. The effect

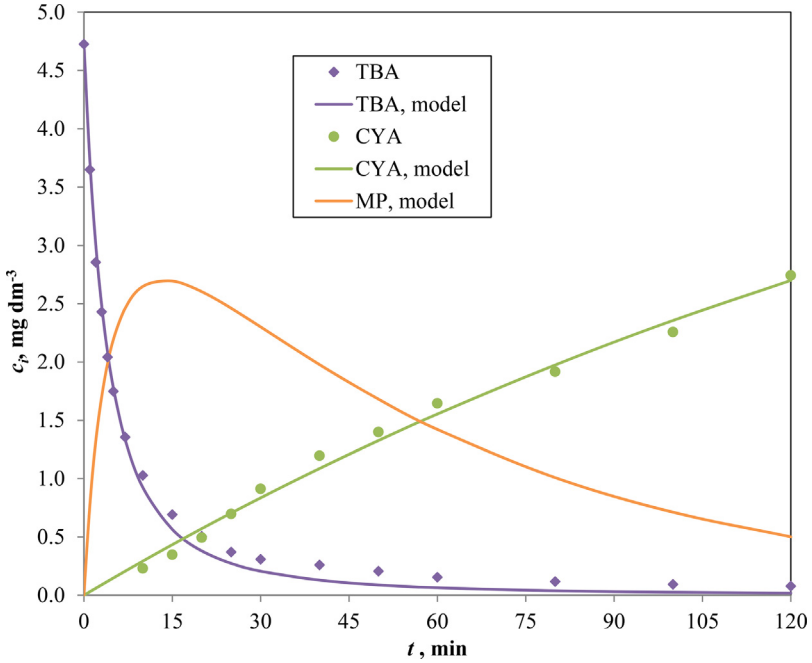

Fig. 12. Fit of experimental data (♦,●) with theoretical data (–) obtained using the model ($c_{(TBA),0}$ = 5 mg L^{-1}, T = 25 °C, Q_R = 300 cm^3 min^{-1}, Q_A = 400 cm^3 min^{-1}, pH = 5, RMSD = 0,015).

Table 4
Values of root mean square deviation R^2, frequency factors, A_r and activation energies, E_a, obtained using UV-C terbuthylazine photocatalysis.

	k_1	k_2
E_a, kJ mol^{-1}	12.88	−0.29
A_r, min^{-1}	0.6725	0.0013
R^2	0.9847	0.9544

of temperature observed during degradation experiments can be caused by its effects on adsorption constants of the reactant and other degradation products, producing the small apparent activation energy [33].

4. Conclusions

The object of this paper was to evaluate the effect of reaction conditions on photocatalytic degradation of terbuthylazine in a closed reaction system with recirculation of the reaction mixture. Experimental data was collected in order to develop and validate the mathematical model. For a better understanding of the degradation pathways, primary degradation products were identified using LC–MS analysis. 6-deisopropylatrazine (DPA), desethylterbuthylazine (DTB), acetamideterbuthylazine (TDA) and hydroxy-terbuthylazine (TBH) were identified and quantified during degradation experiments providing an additional insight to the degradation mechanism. The photolytic degradation of terbuthylazine is quite effective in comparison to photocatalytic degradation of the same component. The major difference between these processes is given with respect to the final product, cyanuric acid. The photolytic process is effective in the hydroxylation process, leading to fast disappearance of terbuthylazine, but hydroxyl radicals are required for an effective dealkylation of side chains. Increasing the recirculation rate of the reaction feed has a positive effect on the degradation resulting in higher final concentrations of cyanuric acid. This can be explained by smaller resistance to the external mass transfer of compounds with thinner boundary layer leading to lower resistance. Increasing the temperature has very small influence on the rate of photocatalysis. A model of the overall reaction system was proposed and developed, including a model of an unsteady annular reactor and a model of the aeration vessel also operating in unsteady conditions. Both parts of system are operating in unsteady conditions because of the time dependency of the concentration in both subsystems, but also due to significant concentration changes along the length of the annular part. The kinetic model is based on a simplified consecutive reaction. The first part of the kinetic model involves the degradation of terbuthylazine and the second part involves the formation of cyanuric acid from the intermediate products. The annular part of the reactor system is usually modelled as a batch reactor. Due to the measured change of concentration along the length of the reactor, the model of the annular reactor is represented by a hyperbolic partial differential equation reduced to an ordinary differential equation by variable substitution. The model of the aeration vessel, which is approximated as the well mixed flow stirred-tank operating in the unsteady state, is given by an ordinary differential equation. The parameters of the overall model were determined by fitting experimental and theoretical data using the Nelder-Mead method of nonlinear optimization. The apparent activation energies and the frequency factors were determined according to Arrhenius law. The model was validated using the measured concentrations of terbuthylazine and cyanuric acid. A very good fit of experimental and theoretical data was obtained. Finally, it can be concluded that the proposed model can be used for a detailed description of the laboratory scale recirculating photocatalytic system containing an immobilized photocatalytic layer.

References

[1] L. Rizzo, Bioassays as a tool for evaluating advanced oxidation processes in water and wastewater treatment, Water Res. 45 (2011) 4311–4340.
[2] S. Malato, P. Fernández-Ibáñez, M.I. Maldonado, J. Blanco, W. Gernjak, Decontamination and disinfection of water by solar photocatalysis: recent overview and trends, Catal. Today 147 (2009) 1–59.
[3] B.K. Avasarala, S.R. Tirukkovalluri, S. Bojja, Photocatalytic degradation of monocrotophos pesticide—An endocrine disruptor by magnesium doped titania, J. Hazard. Mater. 186 (2011) 1234–1240.
[4] C. Chen, S. Yang, Y. Guo, C. Sun, C. Gu, B. Xu, Photolytic destruction of endocrine disruptor atrazine in aqueous solution under UV irradiation: products and pathways, J. Hazard. Mater. 172 (2009) 675–684.
[5] S.G. Botta, D.J. Rodrı'guez, A.G. Leyva, M.I. Litter, Features of the transformation of HgII by heterogeneous photocatalysis over TiO_2, Catal. Today 76 (2002) 247–258.
[6] A. Ayati, A. Ahmadpour, F.F. Bamoharram, B. Tanhaei, M. Mänttäri, M. Sillanpää, A review on catalytic applications of Au/TiO_2 nanoparticles in the removal of water pollutant, Chemosphere 107 (2014) 163–174.
[7] M.A. Sousa, C. Gonçalves, V.J.P. Vilar, R.A.R. Boaventura, M.F. Alpendurada, Suspended TiO_2-assisted photocatalytic degradation of emerging contaminants in a municipal WWTP effluent using a solar pilot plant with CPCs, Chem. Eng. J. (Lausanne) 198–199 (2012) 301–309.
[8] R. Molinari, A. Caruso, P. Argurio, T. Poerio, Degradation of the drugs Gemfibrozil and Tamoxifen in pressurized and de-pressurized membrane photoreactors using suspended polycrystalline TiO_2 as catalyst, J. Membr. Sci. 319 (2008) 54–63.
[9] D. Gumy, S.A. Giraldo, J. Rengifo, C. Pulgarin, Effect of suspended TiO2 physicochemical characteristics on benzene derivatives photocatalytic degradation, Appl. Catal. B 78 (2008) 19–29.
[10] M.S. Nahar, K. Hasegawa, S. Kagaya, Photocatalytic degradation of phenol by visible light-responsive iron-doped TiO_2 and spontaneous sedimentation of the TiO_2 particles, Chemosphere 65 (2006) 1976–1982.
[11] X. Zhang, F. Wu, X. Wu, P. Chen, N. Deng, Photodegradation of acetaminophen in TiO_2 suspended solution, J. Hazard. Mater. 157 (2008) 300–307.
[12] J. Matos, M. Hofman, R. Pietrzak, Synergy effect in the photocatalytic degradation of methylene blue on a suspended mixture of TiO_2 and N-containing carbons, Carbon 54 (2013) 460–471.
[13] L. Ghimici, M. Nichifor, Separation of TiO_2 particles from water and water/methanol mixtures by cationic dextran derivatives, Carbohydr. Polym. 98 (2013) 1637–1643.
[14] T. Szabó, Á. Veres, E. Cho, J. Khim, N. Varga, I. Dékány, Photocatalyst separation from aqueous dispersion using graphene oxide/TiO_2 nanocomposites, Coll. Surf. A 433 (2013) 230–239.
[15] S. Sakohara, R. Hinago, H. Ueda, Compaction of TiO_2 suspension by using dual ionic thermosensitive polymers, Sep. Purif. Technol. 63 (2008) 319–323.
[16] D. Suryaman, K. Hasegawa, S. Kagaya, T. Yoshimura, Continuous flow photocatalytic treatment integrated with separation of titanium dioxide on the removal of phenol in tap water, J. Hazard. Mater. 171 (2009) 318–322.
[17] U.I. Gaya, A.H. Abdullah, Heterogeneous photocatalytic degradation of organic contaminants over titanium dioxide: a review of fundamentals, progress and problems, J. Photochem. Photobiol. C: Photochem. Rev. 9 (2008) 1–12.
[18] L. Reijnders, Hazard reduction for the application of titania nanoparticles in environmental technology, J. Hazard. Mater. 152 (2008) 440–445.
[19] L. Reijnders, Biological effects of nanoparticles used as glidants in powders, Powder Technol. 175 (2007) 142–145.
[20] D.B. Warheit, R.A. Hoke, C. Finlay, E.M. Donner, K.L. Reed, C.M. Sayes, Development of a base set of toxicity tests using ultrafine TiO_2 particles as a component of nanoparticle risk management, Toxicol. Lett. 171 (2007) 99–110.
[21] A. Florence, The oral absorption of micro- and nanoparticulates: neither exceptional nor unusual, Pharm. Res. 14 (1997) 259–266.
[22] L.L.P. Lim, R.J. Lynch, S.-I. In, Comparison of simple and economical photocatalyst immobilisation procedures, Appl. Catal. A 365 (2009) 214–221.
[23] H.D. Mansilla, C. Bravo, R. Ferreyra, M.I. Litter, W.F. Jardim, C. Lizama, J. Freer, J. Fernández, Photocatalytic EDTA degradation on suspended and immobilized TiO_2, J. Photochem. Photobiol. A 181 (2006) 188–194.
[24] S. Parra, S. Elena Stanca, I. Guasaquillo, K. Ravindranathan Thampi, Photocatalytic degradation of atrazine using suspended and supported TiO_2, Appl. Catal. B 51 (2004) 107–116.
[25] S. Mozia, A. Heciak, D. Darowna, A.W. Morawski, A novel suspended/supported photoreactor design for photocatalytic decomposition of acetic acid with simultaneous production of useful hydrocarbons, J. Photochem. Photobiol. A 236 (2012) 48–53.
[26] A. Rachel, M. Subrahmanyam, P. Boule, Comparison of photocatalytic efficiencies of TiO_2 in suspended and immobilised form for the photocatalytic degradation of nitrobenzenesulfonic acids, Appl. Catal. B 37 (2002) 301–308.
[27] G. Mascolo, R. Comparelli, M.L. Curri, G. Lovecchio, A. Lopez, A. Agostiano, Photocatalytic degradation of methyl red by TiO_2: Comparison of the efficiency of immobilized nanoparticles versus conventional suspended catalyst, J. Hazard. Mater. 142 (2007) 130–137.

[28] D. Gumy, A.G. Rincon, R. Hajdu, C. Pulgarin, Solar photocatalysis for detoxification and disinfection of water: different types of suspended and fixed TiO_2 catalysts study, Sol. Energy 80 (2006) 1376–1381.
[29] K. Hashimoto, H. Irie, A. Fujishima, TiO2 photocatalysis a historical overview and future prospects, Jpn. J. Appl. Phys. 44 (2005) 8269–8285.
[30] D. Gumy, C. Morais, P. Bowen, C. Pulgarin, S. Giraldo, R. Hajdu, J. Kiwi, Catalytic activity of commercial of TiO_2 powders for the abatement of the bacteria (E. coli) under solar simulated light: influence of the isoelectric point, Appl. Catal. B 63 (2006) 76–84.
[31] O. Carp, C.L. Huisman, A. Reller, Photoinduced reactivity of titanium dioxide, Prog. Solid State Chem. 32 (2004) 33–177.
[32] K.I. Zamaraev, W. Joe Hightower, et al., Photocatalysis State of the art and perspectives, Stud. Surf. Sci. Catal. Elsevier (1996) 35–50.
[33] J.-M. Herrmann, Photocatalysis fundamentals revisited to avoid several misconceptions, Appl. Catal. B 99 (2010) 461–468.
[34] S.U.M. Khan, M. Al-Shahry, W.B. Ingler, Efficient photochemical water splitting by a chemically modified n-TiO_2, Science 297 (2002) 2243–2245.
[35] G. Liu, L. Wang, H.G. Yang, H.-M. Cheng, G.Q. Lu, Titania-based photocatalysts-crystal growth, doping and heterostructuring, J. Mater. Chem. 20 (2010) 831–843.
[36] M. Ni, M.K.H. Leung, D.Y.C. Leung, K. Sumathy, A review and recent developments in photocatalytic water-splitting using TiO_2 for hydrogen production, Renew. Sustain. Energy Rev. 11 (2007) 401–425.
[37] X. Chen, S.S. Mao, Titanium dioxide Nanomaterials: Synthesis, properties, modifications, and applications, Chem. Rev. 107 (2007) 2891–2959 Washington DC, U.S..
[38] Z. Liu, X. Ge, Y. Lu, S. Dong, Y. Zhao, M. Zeng, Effects of chitosan molecular weight and degree of deacetylation on the properties of gelatine-based films, Food Hydrocoll. 26 (2012) 311–317.
[39] A. Bhatnagar, M. Sillanpää, Applications of chitin- and chitosan-derivatives for the detoxification of water and wastewater — A short review, Adv. Colloid Interface Sci. 152 (2009) 26–38.
[40] W.S.W. Ngah, S.A. Ghani, A. Kamari, Adsorption behaviour of Fe(II) and Fe(III) ions in aqueous solution on chitosan and cross-linked chitosan beads, Bioresour. Technol. 96 (2005) 443–450.
[41] M.A. Nawi, S. Sabar, A.H. Jawad, Sheilatina, W.S.W. Ngah, Adsorption of Reactive Red 4 by immobilized chitosan on glass plates: towards the design of immobilized TiO_2–chitosan synergistic photocatalyst-adsorption bilayer system, Biochem. Eng. J. 49 (2010) 317–325.
[42] M.A. Nawi, S. Sabar, Sheilatina, Photocatalytic decolourisation of Reactive Red 4 dye by an immobilised TiO_2/chitosan layer by layer system, J. Colloid Interface Sci. 372 (2012) 80–87.
[43] J. Le Cunff, V. Tomašić, O. Wittine, Photocatalytic degradation of the herbicide terbuthylazine: preparation, characterization and photoactivity of the immobilized thin layer of TiO_2/chitosan, J. Photochem. Photobiol. A 309 (2015) 22–29.
[44] A. Behnajady Mohammad, E. Siliani-Behrouz, N. Modirshahla, Combination of design equation and kinetic modeling for a batch-recirculated photoreactor at photooxidative removal of C.I. acid red 17, Int. J. Chem. Reactor Eng. 10 (2012).
[45] K. Sopajaree, S.A. Qasim, S. Basak, K. Rajeshwar, An integrated flow reactor-membrane filtration system for heterogeneous photocatalysis. Part II: Experiments on the ultrafiltration unit and combined operation, J. Appl. Electrochem. 29 (1999) 1111–1118.
[46] Y. Sanlaville, S. Guittonneau, M. Mansour, E.A. Feicht, P. Meallier, A. Kettrup, Photosensitized degradation of terbuthylazine in water, Chemosphere 33 (1996) 353–362.
[47] A. Bressan, Hyperbolic Systems of Conservation Laws – The One-dimensional Cauchy Problem, Oxford University Press, Oxford, 2000.